Robustness of Wearable UHF-band PIFAs to Human-Body Proximity

G.A. Casula, A. Michel, P. Nepa,
G. Montisci, and G. Mazzarella

***Abstract*— The robustness of wearable UHF-band planar inverted-F antennas, with respect to body-antenna separation and human tissue dispersion, is addressed through numerical investigations. The main goal is gaining physical insights into the relationship between the grounded antenna performance and the distribution of the electric and magnetic energy densities in the antenna near-field region close to the ground plane border. A criterion for choosing a proper shape of the antenna ground plane is suggested, which can improve the antenna robustness with respect to the random variations of the body-antenna coupling scenario, but with a minimal impact on the antenna size.**

***Index Terms*— body-antenna coupling, grounded antennas, planar inverted-F antennas, wearable antennas.**

I. Introduction

The performance of wearable antennas is significantly modified by the human body proximity [1]-[2]. Moreover, in real-world applications, the antenna-body distance changes randomly, due to the wearer natural movements [3]-[5]. In addition, the electromagnetic and geometrical parameters of the antenna platform (namely, the human body) change from person to person, as well as for different locations of the antenna on the same person, as such parameters vary around the body [6]. The variations of the antenna parameters induced by the above random effects can determine a significant and uncontrolled degradation of the radio link, with respect to the performance expected from an antenna layout optimized to operate at a *nominal* distance from the surface of a *specific* human body phantom. Although a ground plane is effective to minimize the antenna-body coupling effects, it could make the antenna obtrusive and uncomfortable at the UHF-band. In this context, a criterion for choosing a proper shape of the ground plane is desirable to increase the antenna robustness with respect to the random changes of the body-antenna coupling scenario, yet with a minimal impact on the antenna extent. In a number of papers [7]-[11], it has been shown that magnetic antennas can perform better than electric antennas when they operate close to, or inside, the human body (or any other *non-magnetic* lossy material). In the context of wearable and implantable antennas, the best performance of magnetic antennas compared to electric ones is demonstrated mainly for electrically small antennas [7]. Unlike electrically small antennas (where either the electric or the magnetic energy density dominates in the near-field region), resonant antennas exhibit both electric and magnetic energy density peaks. Therefore, it can be expected that a higher reduction of the sensitivity of the antenna parameters to the random changes of the body-antenna coupling scenario can be achieved when the ground plane is elongated at the antenna section characterized by a peak of the electric energy density, rather than at the section close to a peak of the magnetic energy density. A preliminary analysis has been presented in [12].

In this paper, an effort has been made to investigate the performance of Planar Inverted-F Antennas (PIFAs) with different ground plane configurations. A criterion for the selection of the ground plane shape is given, which is based on the position of the maxima of the electric and magnetic energy densities in the antenna near-field region close to the ground plane border. It is worth noting that a discussion on the magnetic and electric energy densities in single-layer antennas was recently introduced in [10], to show that the power loss density in the human body follows the distribution of the electric energy density. However, to the best of the authors' knowledge, this is the first time that the analysis of the distribution of the electric and magnetic energy densities nearby the antenna border is used as a criterion for choosing the shape of the antenna ground plane.

Numerical simulations have been performed using CST Microwave Studio. It is worth noting that all the PIFAs here considered as the initial layouts of our numerical tests have been already adequately tested, both numerically and experimentally, as they have been selected from the open scientific literature.

II. Numerical simulation results

In order to examine the robustness of the antenna behavior with respect to the antenna-body coupling, a set of PIFAs have been numerically analyzed for different ground plane configurations, to investigate for a relationship between their performance and their near-field energy distribution. In particular, results are about two RFID tag antennas operating at 868 MHz [13] and 900 MHZ [14], respectively, and a folded PIFA for on-body communications working at 2.4 GHz [15], so spanning a wide fraction of the UHF spectrum for wearable antenna applications. A numerical phantom has been added to the simulation scenario (Fig. 1) to analyze the body-antenna coupling. We have chosen a three-layer model, composed of a skin layer (1.5 mm thick), a fat layer (20 mm thick), and a muscle layer (30 mm thick).

The radiation efficiency, η, and the power transmission coefficient, τ, have been computed when varying the antenna distance from the human body phantom, d. The radiation efficiency accounts for both the antenna structural losses and the power dissipated into the body model. The power transmission coefficient has been calculated as $\tau = 1 - \left| \left(Z_{IN} - Z^*_0 \right) / \left(Z_{IN} + Z_0 \right) \right|^2$, wherein Z_{IN} is the antenna input impedance, and Z_0 is a reference impedance. Since we

Manuscript received November XX, 2015.

P. Nepa (corresponding author) and A. Michel are with the Department of Information Engineering, University of Pisa, Pisa, Italy (e-mail: [paolo.nepa, andrea.michel] @iet.unipi.it).

G. A. Casula, G. Mazzarella and G. Montisci are with the Dipartimento di Ingegneria Elettrica ed Elettronica, Università di Cagliari, Cagliari, Italy (e-mail: [a.casula, mazzarella]@diee.unica.it, giorgio.montisci@unica.it)

are interested to analyze the robustness of the different layouts with respect to the variations of the antenna-body separation, Z_0 has been assumed equal to the antenna input impedance at the resonance frequency and when d=0 (*i.e.* the antenna adherent to the body model is fully matched to the feeding line, at the resonance frequency). Indeed, an antenna optimization to obtain a specific value for the antenna input impedance (*e.g.* the standard 50 Ω value or the conjugated value of an RFID chip input impedance), at an assigned resonance frequency, is out of the scope of this work.

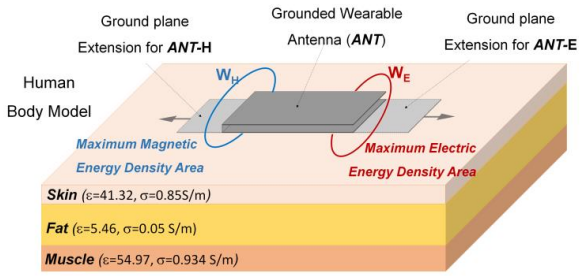

Fig. 1. A PIFA on the phantom model used to perform the numerical investigation of the antenna robustness to the body proximity (the electrical parameters in the figure are those used at 900 MHz). Antenna ground plane can be extended toward either the region with a peak of electric energy density (***ANT-E***) or the region with a peak of magnetic energy density (***ANT-H***).

A reference layout has been selected, which exhibits a ground plane whose size is equal to the size of the antenna radiating element. The reference antenna was named as ***ANT***. Then, the ***ANT*** layout has been modified to get two further configurations:

- ***ANT-E***, in which the ground plane is extended toward the regions close to an electric energy density peak;
- ***ANT-H***, in which the ground plane is extended toward the regions close to a magnetic energy density peak.

The robustness of the configurations ***ANT***, ***ANT*-E**, and ***ANT*-H** with respect to the body-antenna distance d has then been investigated, by analyzing both the variation of the power transmission coefficient τ, and of the power transmission coefficient times the radiation efficiency, $\tau \times \eta$. As a matter of fact, $\tau(d)$ is a decreasing function, since its optimal value (τ=1) is obtained at d=0. On the other hand, η is expected to increase, on average, with d. From the point of view of the system, $\tau \times \eta$ is the main determinant of the link budget, but also τ is separately of interest, since a significant mismatch can damage the transmitter or reduce the signal-to-noise level at the receiver. Therefore, the robustness of the proposed configurations has been studied separately for τ and $\tau \times \eta$, and the best ground plane configuration is considered to be that one exhibiting a reasonable value of $\tau \times \eta$, with a τ as great as possible, with both stable with respect to the antenna-body distance, d. In the following, it is assumed that the variations of the antenna directivity and radiation pattern are negligible, as the set of body-antenna separations here considered are very small with respect to the wavelength.

A. *Wearable Planar Inverted-F Antenna at 868MHz*

The first example is about an antenna suitable for wearable tags at 868 MHz [13]. In this case, in order to obtain a reference antenna (***ANT***), the original configuration proposed in [13] has been modified reducing the ground plane size to exactly fit the radiating patch dimension (Fig. 2). The geometrical parameters used in the numerical simulations are summarized in Fig. 2c, and the electric and magnetic energy densities are shown in Fig. 2d and Fig. 2e, respectively.

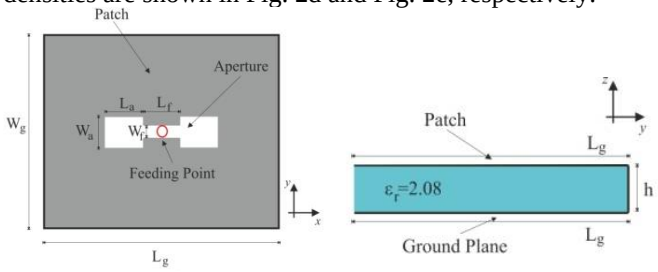

(a) (b)

Antenna Parameters, [mm]						
W_g	L_g	W_a	L_a	W_f	L_f	h
49	60	8	10	3	10	4

(c)

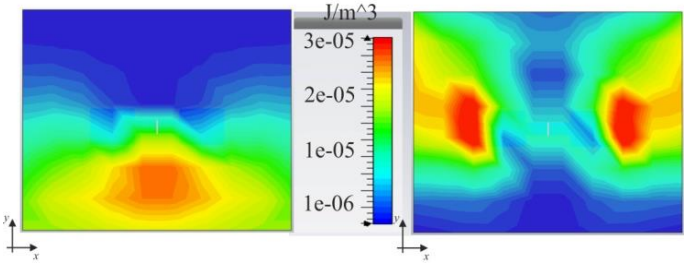

(d) (e)

Fig. 2. Front view (a), lateral view (b), and main geometrical parameters of the considered layout (c) for the ***ANT*** configuration (PIFA in [13]). For such a structure, the electric (d) and magnetic (e) energy densities are shown close to the ground plane, at the resonant frequency.

The electric energy density shows a single peak, close to the antenna open end, whereas the magnetic energy density shows two peaks, each one close to the antenna lateral edges. Two modified layouts have been obtained by adding an extension of the ground plane toward the direction where the peaks of the electric and magnetic energy density appear, respectively: ***ANT-E*** configuration, with a ground plane extension ΔL_E (Fig. 3a), and ***ANT-H*** configuration, with a ground plane extension ΔL_H (Fig. 3b). The size of ΔL_E and ΔL_H (which should be as small as possible in order to obtain a wearable antenna that is unobtrusive, compact, and comfortable to the user) has been searched through a local tuning. In Fig. 4, the power transmission coefficient τ for the antennas ***ANT***, ***ANT-E***, ***ANT-H*** (Figs. 2 and 3), and the reference antenna in [15], is shown for d=0 (antenna attached to the body). The usable bandwidth of all these configurations is satisfactory, and covers the typical frequency band requested to UHF RFID applications. For the antennas ***ANT***, ***ANT-E*** and ***ANT-H***, numerical results for the input impedance, Z_{IN}, and the radiation efficiency, η, have been obtained at the resonant

frequency, when the body–antenna separation, *d*, varies from 0 up to 15 mm. Hence, the product between the power transmission coefficient, τ, and the radiation efficiency η has been computed for each of the three antenna layouts.

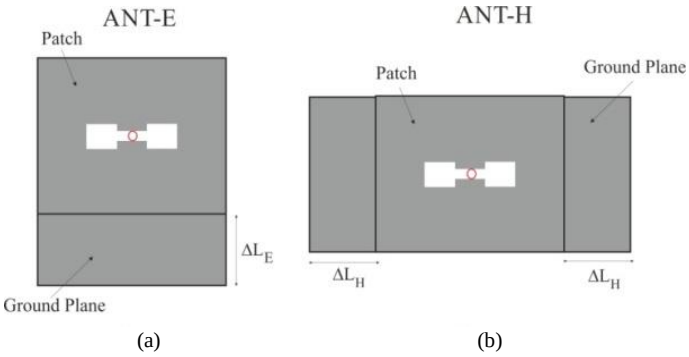

Fig. 3. PIFA in [13] with an extended ground plane: ***ANT-E*** (a); ***ANT-H*** (b).

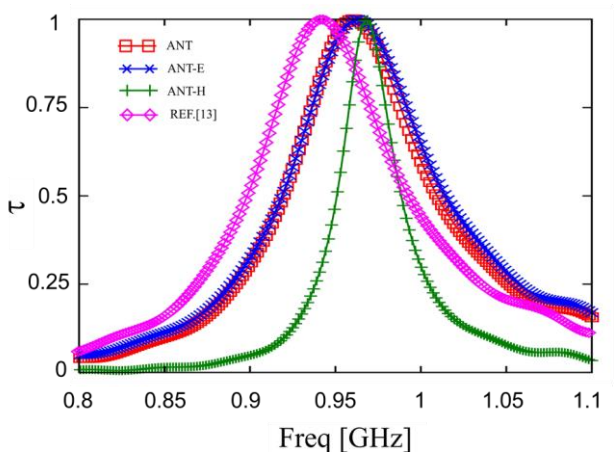

Fig. 4. Power transmission coefficient of the antennas **ANT**, **ANT-E** (ΔL_E = 30 mm), **ANT-H** (ΔL_H = 30 mm) (Figs. 2 and 3), and for the reference antenna in [13], computed for d = 0 (antenna attached to the body).

The variation against *d* of τ and ($\tau \times \eta$) is shown in Fig. 5a and 5b, respectively, for the antennas ***ANT***, ***ANT-E***, ***ANT-H***, and for the reference antenna in [13]. For the ***ANT-E*** and ***ANT-H*** configurations, the results for three different values of ΔL_E and ΔL_H are shown. The best performance is obtained for ΔL_E = 30 mm and ΔL_H = 30 mm. These results clearly indicate that the ***ANT-E*** configuration performs better. The robustness of the ***ANT-E*** with respect to the body-antenna distance variation is remarkable when compared to the reference antenna.

In order to test the robustness of the proposed configurations also with respect to the frequency, the variation of τ and $\tau \times \eta$ for the ***ANT***, ***ANT-E*** (for ΔL_E = 30 mm) and ***ANT-H*** (for ΔL_H = 30 mm) configurations is shown in Fig 6, for three different frequencies: the resonant frequency f_0, and the frequencies f_0-*10 MHz* and f_0+*10 MHz*. Again, it is apparent that the ***ANT-E*** configuration results the more robust with respect to the body-antenna separation.

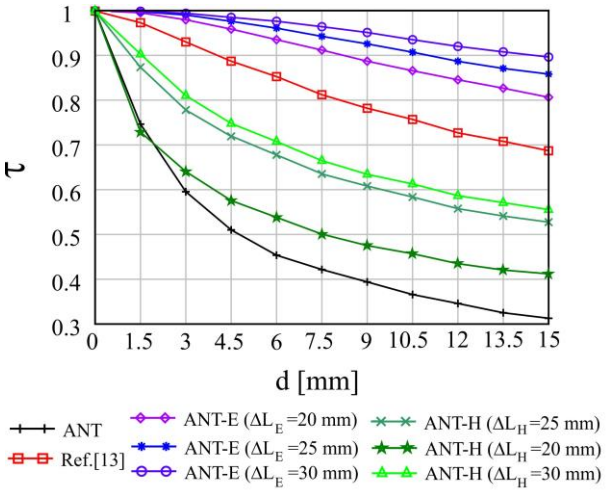

(a)

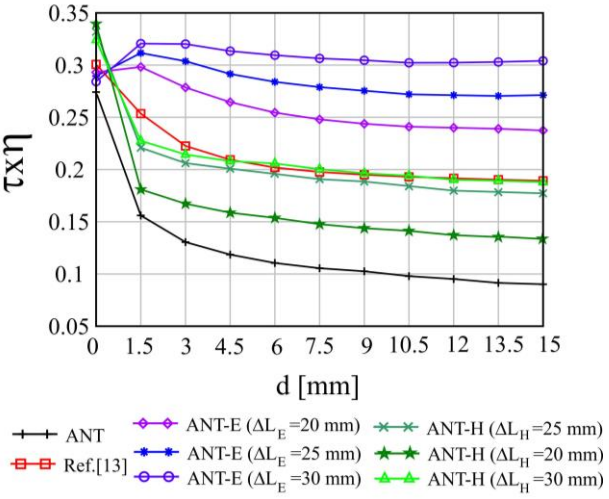

(b)

Fig. 5. Variation of τ (a), and of the product $\tau \times \eta$ (b), for the ***ANT***, ***ANT-E***, ***ANT-H*** antennas (Figs. 2 and 3), and for the reference antenna in [13].

B. Wearable Planar Inverted-F Antenna at 900MHz

The above analysis has been repeated for a PIFA-type tag antenna working at 900 MHz [14]. The original configuration proposed in [14] (and reported in Fig.7) has been modified by reducing the ground plane size to exactly fit the radiating patch dimension (Wg=Wp and Lg=Lp), to get the reference antenna ***ANT***. The geometrical parameters used in the numerical simulations are summarized in Fig. 7d, and the electric and magnetic energy densities are shown in Fig. 7e and Fig. 7f, respectively. The maximum of the electric energy density is close to the antenna open end, whereas the maximum of the magnetic energy density is close to the antenna shorting edge, as expected.

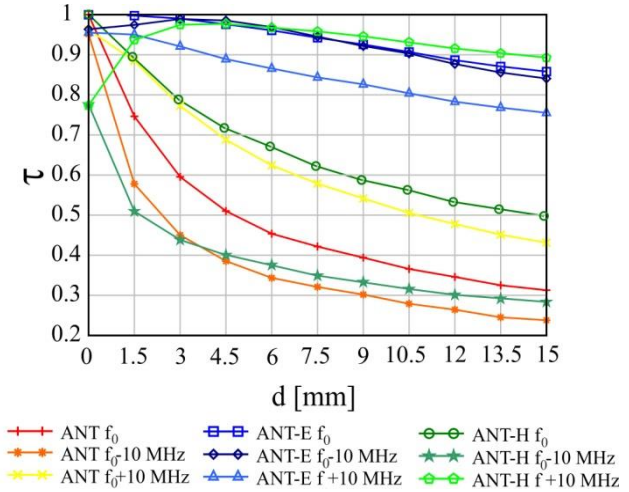

(a)

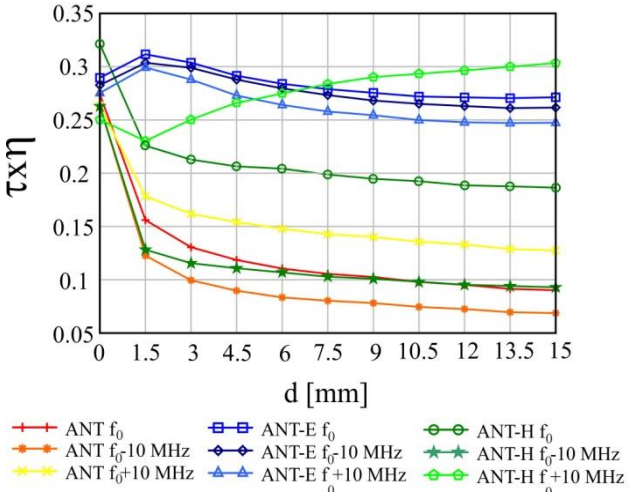

(b)

Fig. 6. Variation of τ (a), and of the product $\tau \times \eta$ (b), for the ***ANT***, ***ANT-E*** and ***ANT-H*** antennas (Figs. 2 and 3), evaluated for three different frequency values. ΔL_E = 30 mm, ΔL_H = 30 mm.

The modified layouts obtained by adding an extension of the ground plane toward the direction where the peak of the electric or magnetic energy density appears, are shown in Fig. 8a (***ANT-E*** configuration) and in Fig. 8b (***ANT-H*** configuration). In Fig. 9, the variation against *d* of τ (Fig. 9a) and τ × η (Fig. 9b) is shown for the ***ANT***, ***ANT-E***, and ***ANT-H*** configurations. The optimal values of the ground plane extensions are ΔL_E = 35 mm and ΔL_H = 36 mm. Again, the robustness of the ***ANT-E*** configuration with respect to the body-antenna distance variation is apparent, whereas the ***ANT-H*** configuration presents only a negligible improvement with respect to the ***ANT*** configuration.

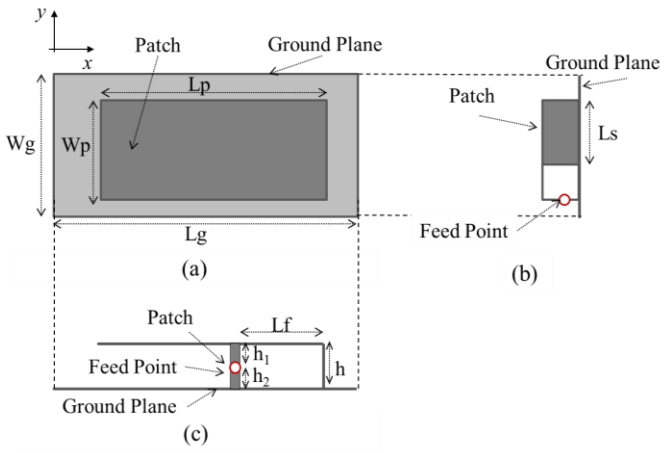

Antenna Parameters, [mm]								
W_g	**L_g**	**W_p**	**L_p**	**L_s**	**L_f**	**h**	**h1**	**h2**
40	70.5	40	70.5	24	17.5	3	2.465	0.1

(d)

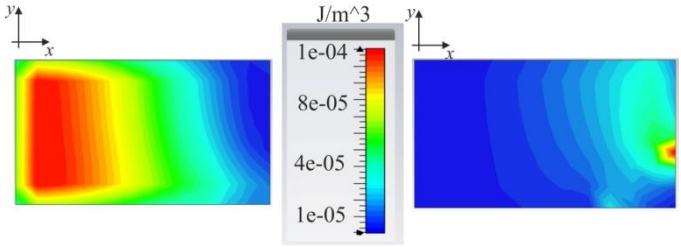

(e) (f)

Fig. 7. Top view (a), side view (yz plane) (b), side view (xz plane) (c), and main geometrical parameters of the ***ANT*** configuration [14] (d), for the PIFA in [14]. For such a structure, the electric (e) and magnetic (f) energy densities are shown close to the ground plane, at the resonant frequency.

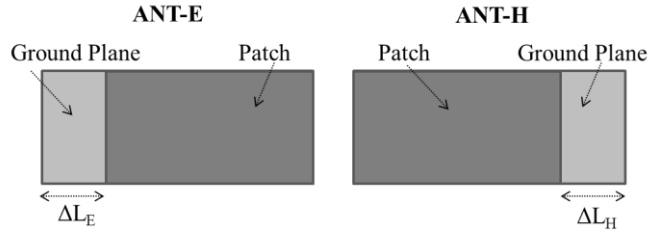

(a) (b)

Fig. 8. PIFA [14] with the ground plane extended toward the open-end (**ANT-E**) (a); PIFA [14] with the ground plane extended toward the shorting-edge (**ANT-H**) (b).

C. PIFA antenna at 2.4 GHz

As a last example, a folded PIFA for on-body communications at 2.4 GHz is considered [15]. In this case, the reference antenna layout (***ANT***) is identical to the original configuration presented in [15]. Fig. 10b describes the geometrical parameters used in the numerical simulations, and the electric and magnetic energy densities are shown in Fig. 10c and Fig. 10d, respectively.

The magnetic energy density shows a single peak, close to the antenna shorting edge, whereas the electric energy density shows two peaks, each one close to the antenna lateral edges. The modified layouts obtained by adding an extension of the ground plane toward the peaks of the electric and magnetic energy density, are shown in Fig. 11a (***ANT-E*** configuration) and in Fig. 11b (***ANT-H*** configuration), respectively.

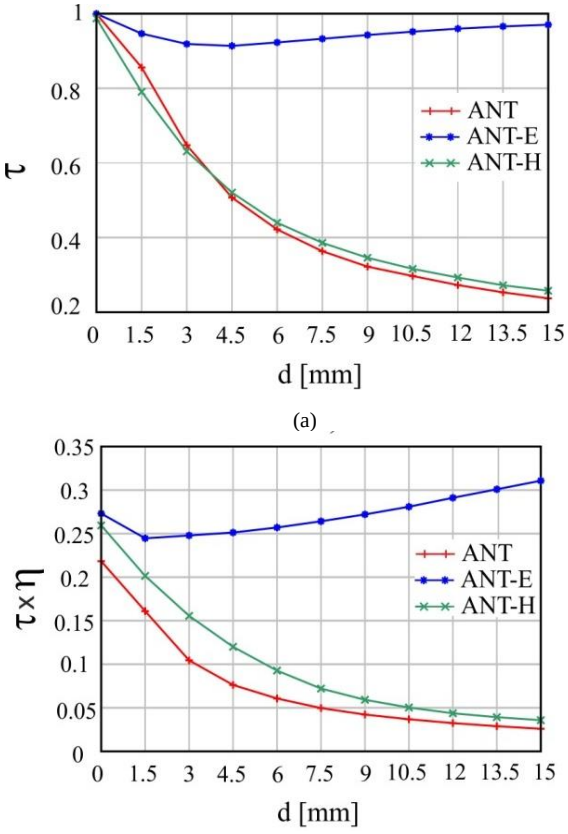

Fig. 9. Variation of τ (a), and of the product $\tau \times \eta$ (b), for the ***ANT***, ***ANT-E***, ***ANT-H*** antennas (Figs. 7 and 8). ΔL_E = 35 mm, ΔL_H = 36 mm.

In Fig. 12, the variation of τ (Fig. 12a) and $\tau \times \eta$ (Fig. 12b) is shown for ***ANT***, ***ANT-E***, and ***ANT-H*** configurations. Again, this further example confirms that the robustness of the ***ANT-E*** configuration with respect to the body-antenna distance variation is significantly better than the other configurations (i.e, ***ANT*** and ***ANT-H***). It is important to highlight that, notwithstanding the percentage variations of $\tau \times \eta$ (Fig. 12b) seem comparable for all the analyzed configurations, the percentage variation of τ (Fig. 12a) is unacceptable for both ***ANT*** and ***ANT-H*** configurations. This means that, for both ***ANT*** and ***ANT-H***, τ and η vary in a larger interval, but in opposite directions (τ decreases with d up to 25%, whereas η increases with d up to 90%). For the ***ANT-E*** configuration τ and η show the same behavior, but the variations are small (τ decreases with d up to 5%, whereas η increases with d up to 40%). Moreover, the value of $\tau \times \eta$ is definitely larger for the ***ANT-E*** configuration.

For all the antennas investigated in this paper, the variation of τ and $\tau \times \eta$ has also been calculated when the permittivity and conductivity of the phantom layers are changed. However, when considering variations of the permittivity and conductivity of the numerical phantom layers up to +/-15%, numerical results for τ and η have shown quite small variations (less than 1%), so resulting negligible with respect to those induced by the antenna-body distance.

The results here presented showed that, to increase the robustness of a PIFA antenna with respect to the body-antenna separation variations, the ground plane should be extended in the direction corresponding to the antenna border close to an electric energy density peak. Such a conclusion agrees with previous results on electrically small antennas [7]-[11], which state that electric antennas perform worse than magnetic antennas, when they operate next to or inside the human body.

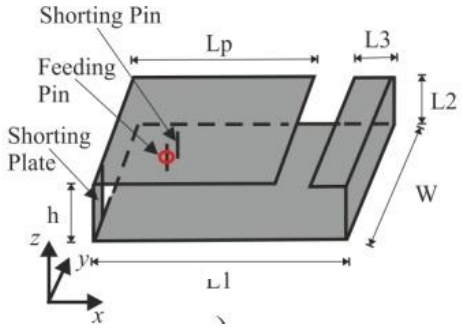

Antenna Parameters, [mm]					
L_1	**L_2**	**L_3**	**W**	**L_p**	**h**
26	3.5	2.5	26	20.5	3.5

(b)

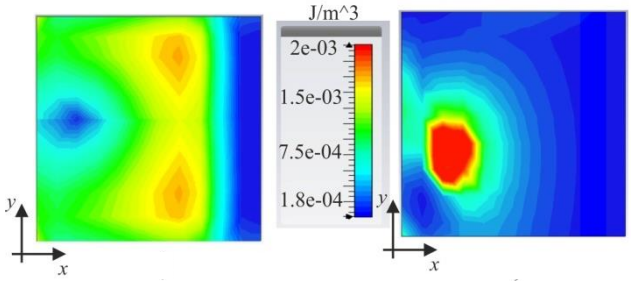

Fig. 10. Three-dimensional view (a), and main geometrical parameters (b) of the considered layout for the ***ANT*** configuration, for antenna in [15]. For such a structure, the electric (c) and magnetic (d) energy densities are shown close to the ground plane, at the resonant frequency.

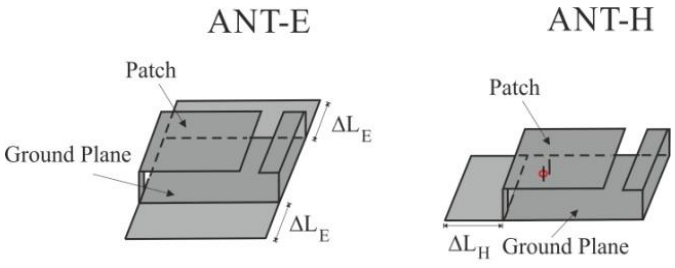

Fig. 11. PIFA antenna in [15] with the ground plane extended toward the directions of the maxima of the electric energy density (ANT-E) (a); PIFA antenna with the ground plane extended toward the shorting-edge (ANT-H) (b).

III. Conclusion

The robustness of a set of Planar Inverted-F antennas to the random variations induced by the body-antenna separation and human tissue dispersion has been numerically investigated, by relating it to the electric and magnetic energy density distributions in the antenna near-field region around the ground plane border. Based on the presented examples, we can conclude that ground plane enlarging is more effective at those sections of the antenna border where the electric energy density exhibits a peak. Such a design guideline can be used as a physics-based criterion in order to reduce the computational efforts required by a brute-force numerical optimization of the PIFA ground plane size and shape. Nevertheless, the proposed design approach may be applied to other grounded antennas for body-centric communications, yet limited to those antennas exhibiting a small variation of the energy density distributions within their operative frequency band.

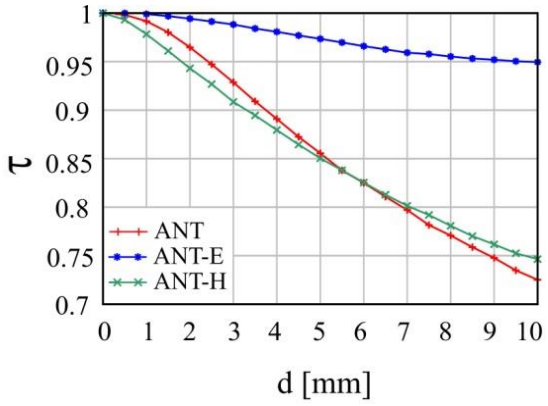

(a)

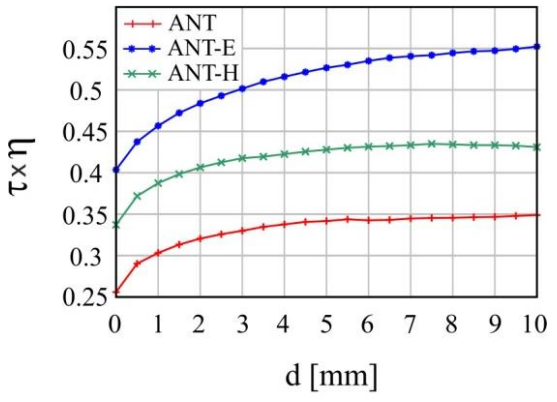

(b)

Fig. 12. Variation of τ (a), and of the product $\tau \times \eta$ (b), for the ***ANT***, ***ANT-E***, ***ANT-H*** antennas (Figs. 10 and 11). ΔL_E = 15 mm, ΔL_H = 15 mm.

References

[1] P. Nepa and H. Rogier, "Wearable antennas for off-body radio links at VHF and UHF bands (below 1 GHz): challenges, state-of-the-art and future trends," *IEEE Antennas and Propagation Magazine*, vol. 57, n. 5, pp. 1-23, 2015.

[2] P.S. Hall, Y. Hao, V.I. Nechayev, A. Alomainy, C.C. Constantinou, C. Parini, M.R. Kamarudin, T.Z. Salim, D.T.M. Heel, R. Dubrovka, A.S. Owadall, W. Song, A.A. Serra, P. Nepa, M. Gallo and M. Bozzetti, "Antennas and Propagation for On-Body Communication Systems", *IEEE Antennas and Propagation Magazine*, vol. 49(3), pp. 41–58, 2007.

[3] A. Serra, P. Nepa, and G. Manara, "A wearable two-antenna system on a life jacket for Cospas-Sarsat Personal Locator Beacons," *IEEE Trans. on Antennas and Propagation*, 60 (2), part II, pp. 1035-1042, 2012.

[4] P. Nepa and G. Manara, "On the Stochastic Characterization of Wearable Antennas," *PIERS 2013*, Stockholm, Sweden, 12-15 August, 2013.

[5] A. Baroni, P. Nepa and H. Rogier, "Wearable self-tuning antenna for emergency rescue operations", IET Microwaves, Antennas & Propagation Microwaves, vol. 10, n. 10, pp. 173-183, 2016.

[6] A. Michel, K. Karathanasis, P. Nepa and J.L. Volakis, "Accuracy of a Multi-probe Conformal Sensor in Estimating the Dielectric Constant in Deep Biological Tissues," *IEEE Sensor Journal*, vol. 15, n.9, pp. 5217-5221, 2015.

[7] F. Merli, B. Fuchs, J.R. Mosig, and A.K. Skrivervik, "The effect of insulating layers on the performance of implanted antennas, *IEEE Trans. on Antennas and Propagation*, 59(1), pp. 21-31, January 2011.

[8] W. Scanlon and N. Evans, "Antennas and propagation for telemedicine and healthcare: on-body systems," in *Antennas And Propagation for Body-Centric Wireless Communications*, Edited by P.S. Hall and Y. Hao, Artech House Inc., Norwood, MA, 2006, , Ch. 8: pp. 211-239.

[9] M. Manteghi and A.A.Y. Ibraheem, "On the study of the Near-Fields of Electric and Magnetic Small Antennas in Lossy Media," *IEEE Trans. on Antennas and Propagation*, vol. 62 (12), pp. 6491-6495, December 2014.

[10] R. M. Makinen, T. Kellomaki, "Body effects on thin single-layer slot, self-complementary, and wire antennas," *IEEE Transactions on Antennas and Propagation*, vol. 82(1), pp. 385-392, January 2014.

[11] J. Trajkovikj and A.K. Skrivervik, "Dimishing SAR for wearable UHF antennas," *IEEE Antennas and Wireless propagation Letters*, pp. 1-4, 2014

[12] M. Altini, G.A. Casula, G. Mazzarella, and P. Nepa, "Numerical investigation on the tolerance of wearable UHF-RFID tags to human body coupling", *IEEE 2015 Antennas and Propagation Symposium*, Vancouver, BC, Canada, July 20-24, 2015.

[13] C. Occhiuzzi, S. Cippitelli, and G. Marrocco, "Modeling, design and experimentation of wearable RFID sensor tag", *IEEE Trans. Antennas Propagation*, 58(8), pp. 2490–2498, 2010.

[14] M.-H. Lin and C.-W. Chiu "Human-body effects on the designof card-type UHF RFID tag antennas", Proc. IEEEAP-S Int. Symp., pp.521 - 524 2011

[15] C.-H. Lin, K. Saito, M. Takahashi, and K. Ito, "A compact planar inverted-F antenna for 2.45 GHz on-body communications," *IEEE Transactions on Antennas and Propagation*, vol. 60, no. 9, pp. 4422-4426, 2012.